Editors' Suggestion

Bath-Engineering Magnetic Order in Quantum Spin Chains: An Analytic Mapping Approach

Brett Min,[1,*] Nicholas Anto-Sztrikacs,[1] Marlon Brenes,[1] and Dvira Segal[2,1,†]
[1]*Department of Physics and Centre for Quantum Information and Quantum Control, University of Toronto, 60 Saint George Street, Toronto, Ontario, M5S 1A7, Canada*
[2]*Department of Chemistry, University of Toronto, 80 Saint George Street, Toronto, Ontario, M5S 3H6, Canada*

(Received 15 January 2024; revised 22 March 2024; accepted 15 May 2024; published 24 June 2024)

Dissipative processes can drive different magnetic orders in quantum spin chains. Using a nonperturbative analytic mapping framework, we systematically show how to structure different magnetic orders in spin systems by controlling the locality of the attached baths. Our mapping approach reveals analytically the impact of spin-bath couplings, leading to the suppression of spin splittings, bath dressing and mixing of spin-spin interactions, and emergence of nonlocal *ferromagnetic* interactions between spins coupled to the same bath, which become long ranged for a global bath. Our general mapping method can be readily applied to a variety of spin models: we demonstrate (i) a bath-induced transition from antiferromagnetic (AFM) to ferromagnetic ordering in a Heisenberg spin chain, (ii) AFM to extended Neel phase ordering within a transverse-field Ising chain with pairwise couplings to baths, and (iii) a quantum phase transition in the fully connected Ising model. Our method is nonperturbative in the system-bath coupling. It holds for a variety of non-Markovian baths and it can be readily applied towards studying bath-engineered phases in frustrated or topological materials.

DOI: 10.1103/PhysRevLett.132.266701

Introduction.—Spin chains offer a versatile platform for the study of quantum materials. They can capture a wide range of complex and exotic phenomena from magnetic effects to topological phases. These effects are observed in a variety of materials, including quantum magnets, spin liquids, and quantum wires. Beyond ideal models, in reality, environmental degrees of freedom such as lattice phonons or engineered cavity modes couple to the spin degrees of freedom. The resulting decoherence and dissipative effects may largely impact magnetic ordering in spin systems, even inducing quantum phase transitions, effects that stem from the interplay between internal spin-spin interactions and dissipation [1–46]. These demonstrations were done using numerical approaches, facilitated by analytical arguments. The behavior of a collection of spins coupled to a *common* (global) bosonic bath was studied in Refs. [1–16], where it was demonstrated, using techniques such as the numerically exact quantum Monte Carlo method [1–4], that such models can exhibit dissipation-controlled quantum phase transition. Other numerical studies focused on chains with sites *independently* (locally) coupled to dissipative baths [4–6,17–43,47–49] demonstrating, e.g., long-range antiferromagnetic order at any coupling to the baths in an antiferromagnetic quantum Heisenberg chain. Alternatively, other studies were done in the premise of weak system-bath couplings and/or structureless dissipation using, e.g., the Lindblad quantum master equation [5,6,12–15,33–45]. While numerical studies of bath-controlled spin phases were often accompanied by analytical arguments; a rigorous, unified, and general analytic framework to bath-controlled phases is still missing.

Here, we show that a general mapping approach can be used to study a broad class of open spin systems and provide an intuitive, *unified*, and comprehensive understanding of bath-induced phase transitions. Our method can treat global, local, or partially local spin-bath coupling schemes at finite temperature and different families of baths' spectral density functions. The method is nonperturbative in the spin-bath coupling, thus enabling the capture of effects emerging from strong-coupling many-body physics. In a nutshell, based on unitary transformations and a controlled truncation, the mapping turns the spin + baths Hamiltonian into an *effective* Hamiltonian with the spin system now *weakly* coupled to its environments. Most crucially, our mapping approach reveals the generation of bath-mediated spin-spin interactions, which extend beyond nearest-neighboring spins—depending on the nonlocality of the attached baths. Here, the dissipative system favors a ferromagnetic order, the result of our specific choice of the interaction model. The mapping, however, is not limited to generating only ferromagnetic interactions. Bath-induced effects further mix and dress the intrinsic spin-spin couplings and suppress spin splittings. Through these bath-induced effects, our *closed-form*, Hermitian, effective spin Hamiltonian immediately evinces on the expected magnetic order as one tunes the system's couplings to its surroundings.

After discussing the mapping approach, we apply it on several spin models coupled globally or locally to different non-Markovian baths (super-Ohmic, Brownian) and examine their equilibrium phases as a function of system-bath couplings at low temperature.

Mapping.—We consider a many-body system described by the Hamiltonian $\hat{H}_S$ coupled to a bosonic-harmonic environment. For simplicity, we describe the mapping in a model with a single heat bath. The total Hamiltonian of the system, environment, and their interaction reads

$$\begin{aligned}\hat{H} &= \hat{H}_S + \hat{H}_B + \hat{H}_I \\ &= \hat{H}_S + \sum_k \nu_k \hat{c}_k^\dagger \hat{c}_k + \hat{S}\sum_k t_k(\hat{c}_k^\dagger + \hat{c}_k), \end{aligned} \tag{1}$$

where $\hat{c}_k^\dagger(\hat{c}_k)$ are bosonic creation (annihilation) operators with frequency ν_k for the kth harmonic mode. $\hat{S}$ is an operator defined over the system's degrees of freedom, which couples to the reservoir with a coupling strength captured by the bath spectral density function, $K(\omega) = \sum_k t_k^2 \delta(\omega - \nu_k)$.

An "effective" Hamiltonian can be constructed by sequentially applying the reaction coordinate and polaron transformations onto the total Hamiltonian Eq. (1), followed by a controlled truncation [50–52]. This mapping is defined such that the coupling of the system to the reservoir is made weaker in the new picture, while the effects of strong system-bath couplings are absorbed into the effective system's Hamiltonian [53]. Post mapping, the effective (eff) Hamiltonian reads $\hat{H}^{\rm eff} = \hat{H}_S^{\rm eff}(\lambda, \Omega) + \hat{H}_B^{\rm eff} + \hat{H}_I^{\rm eff}$, and we highlight the dependence of the effective system's Hamiltonian on λ and Ω. These parameters are functions of the original spectral function of the bath, $K(\omega)$ [52]. They can be interpreted as a system-bath interaction energy scale (λ) and a characteristic frequency (Ω) of the bath, both corresponding to the original bath described in Eq. (1). The effective system couples to a modified (residual) bath $\hat{H}_B^{\rm eff} = \sum_k \omega_k \hat{b}_k^\dagger \hat{b}_k$ through $\hat{H}_I^{\rm eff} = -(2\lambda/\Omega)\hat{S}\sum_k f_k(\hat{b}_k^\dagger + \hat{b}_k)$; $\hat{b}_k^\dagger(\hat{b}_k)$ corresponds to new bosonic creation (annihilation) operators with frequency ω_k. Importantly, a κ scaling of the original coupling, $\kappa K(\omega)$, does not impact the spectral function of the residual bath, $K^{\rm RC}(\omega) = \sum_k f_k^2 \delta(\omega - \omega_k)$ [50–53]; the spectral function $K^{\rm eff}(\omega) = (4\lambda^2/\Omega^2)K^{\rm RC}(\omega)$ characterizes the redefined bath. The parameters for the original bath spectral function are chosen to ensure weak residual coupling, described by $K^{\rm eff}(\omega)$. The scaling observation allows building effective models in which the residual bath only weakly couples to the system [52]. This allows us to compute the system's equilibrium state resulting from its interaction with the bath as the Gibbs state with respect to the *effective* system's Hamiltonian, $\rho_S^{\rm eff} = (1/Z^{\rm eff})e^{-\beta \hat{H}_S^{\rm eff}}$; $Z^{\rm eff} = {\rm Tr}[e^{-\beta \hat{H}_S^{\rm eff}}]$ is the partition function with β the inverse temperature of the bath [54–56]. This approach was successfully validated on impurity models [50,51], and it is utilized here as a general analytical method for tailoring magnetic order in open quantum lattices.

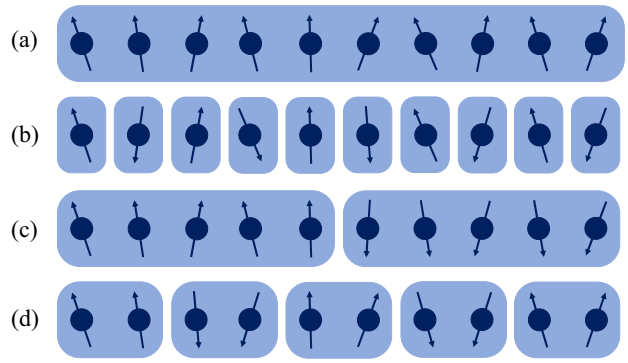

FIG. 1. Models for spin-1/2 chains coupled to independent reservoirs, whose range of interaction is depicted by the light blue shades over the spins. (a) Fully global model: the entire chain is coupled to the same bath. (b) Fully local case: individual spins are coupled to their own local bath. (c),(d) Intermediate bath-locality models: each bath couples to more than a single spin with, e.g., (c) half-and-half coupling and (d) pairwise coupling.

Spin chains.—The dissipative Heisenberg chain with N sites is given by Eq. (1), with the system's Hamiltonian

$$\hat{H}_S = \sum_{i=1}^{N} \Delta_i \hat{\sigma}_i^z + \sum_\alpha \sum_{i=1}^{N-1} J_\alpha \hat{\sigma}_i^\alpha \hat{\sigma}_{i+1}^\alpha. \tag{2}$$

Here, $\Delta_i > 0$ represents the spin splitting of the ith spin. We set $J_\alpha > 0$ as the uniform interaction strength between neighboring spins in the $\alpha = \{x, y, z\}$ direction. We consider four scenarios, depicted in Fig. 1: (a) *fully global* and (b) *fully local* baths, as well as (c) *half-and-half* and (d) *pairwise* coupling schemes. Cases (a) and (d) are presented here; the other two models can be found in Ref. [52].

We implement two complementary mapping procedures on spin chains [52]: (i) we build on the reaction coordinate mapping to adjust the system-bath boundary, followed by a polaron rotation of the reaction coordinate and its truncation [50,51]. (ii) We apply a polaron rotation *directly* on the interaction Hamiltonian, acting on all modes in the bath. We show in Ref. [52] that the two mapping methods build completely analogous system's Hamiltonian $\hat{H}_S^{\rm eff}$, along with a weakened system-bath coupling strength. For equilibrium properties, the two approaches thus provide parallel results [51]; deviations may show in time-dependent simulations. Conceptually, the methods can each handle general spectral density functions, yet it is convenient to enact the first (i) mapping method on a Brownian bath with $K(\omega) = 4\gamma\Omega^2\lambda^2\omega/[(\omega^2 - \Omega^2)^2 + (2\pi\gamma\Omega\omega)^2]$; λ is the system-bath coupling energy and the bath is peaked at Ω with width energy $\gamma\Omega$. In the effective picture, $K^{\rm eff}(\omega) \propto \gamma\omega$ [57], thus the system-bath interaction in $H^{\rm eff}$ becomes

weak once $\gamma \ll 1$. The second mapping (ii) can be readily performed on the Ohmic family spectral functions, e.g., $K(\omega) = \alpha(\omega^3/\omega_c^2)e^{-\omega/\omega_c}$ with α a dimensionless coupling parameter. Under the polaron picture [58], the parameters λ and Ω that are used to define the effective system Hamiltonian can be expressed in terms of α and ω_c [52].

Fully global coupling.—The Hamiltonian is given by Eq. (1) with the Heisenberg Hamiltonian Eq. (2). In the fully global coupling model, all the spins couple to a single bath and we use as an example the interaction operator $\hat{S}_{\rm glob} = \sum_{i=1}^{N} \hat{\sigma}_i^x$. The mapped system is given by [52]

$$\hat{H}^{\rm eff}_{{\rm glob},S} = \sum_{i=1}^{N} \tilde{\Delta}_i \hat{\sigma}_i^z + \sum_{\alpha} \sum_{i=1}^{N-1} \tilde{J}_\alpha \hat{\sigma}_i^\alpha \hat{\sigma}_{i+1}^\alpha - \frac{\lambda^2}{\Omega} \hat{S}^2_{\rm glob}, \quad (3)$$

with $\tilde{\Delta}_i = \Delta_i e^{-(2\lambda^2/\Omega^2)}$, $\tilde{J}_x = J_x$, and spin interactions renormalized according to $\tilde{J}_{y(z)} = (J_{y(z)}/2)(1 + e^{-(8\lambda^2/\Omega^2)}) + (J_{z(y)}/2)(1 - e^{-(8\lambda^2/\Omega^2)})$. First, as expected, $\hat{H}^{\rm eff}_{{\rm glob},S} \to \hat{H}_S$ as $\lambda \to 0$. Second, environmental effects on the magnetic order at low temperature are transparent in this picture: As a function of λ, with our particular choice of $\hat{S}_{\rm glob}$ (which the mapping is not limited to), the effect of the environment is to mix the anisotropies with respect the x component, i.e., the y and z components. Furthermore, the individual spin splittings Δ_i are exponentially suppressed as λ increases. This suppression can be rationalized as the entire chain is coupled in the x direction, which leads to spins aligning in that direction as the coupling strength increases. One can imagine an analogous scenario of turning on a strong magnetic field in the x direction, which would similarly suppress spin components in the z direction. Most dramatically, the last term in Eq. (3) describes all-to-all spin interactions arising in the x direction at nonzero λ, favoring ferromagnetic order in the present choice of system-bath interaction model. For later use, we denote this energy by $E_I \equiv (\lambda^2/\Omega)$. In the super-Ohmic model, it is given by $E_I \equiv 2\alpha\omega_c$ [52]. On physical grounds, this term with its accompanied minus sign is to be expected since the spin chain is coupled to a common environment [59]. Recall that λ and Ω can be derived for distinct baths' spectral density functions, ensuring the versatility of the mapping.

Corroborating these observations, deduced from Eq. (3), in Fig. 2 we simulate the structure factor $S_\alpha = (1/N^2)\sum_{ij}\langle \hat{\sigma}_i^\alpha \hat{\sigma}_j^\alpha \rangle$ for a Heisenberg chain with N spins. The thermal average is done over the density matrix built from the effective Hamiltonian of the system, $\hat{H}^{\rm eff}_{{\rm glob},S}$. The structure factor manifests a clear crossover with increasing λ, from the antiferromagnetic (AFM) alignment of spins due to $J_\alpha > 0$, to a FM order in the x direction, with S_x going from a value close to zero, to approaching 1 [Fig. 2(a)]. Furthermore, S_z (and similarly S_y, not shown) demonstrate that all correlations in the z (and y) directions are suppressed,

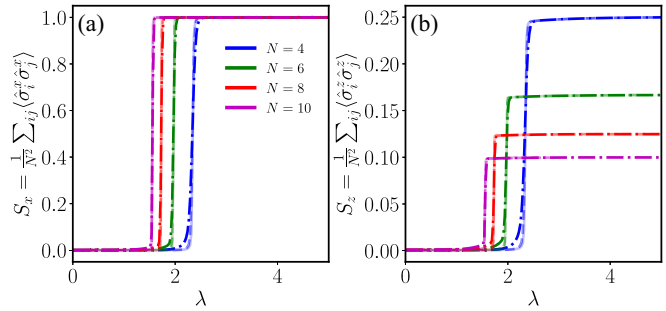

FIG. 2. Heisenberg spin chain in a global bath. We display the structure factors $S_\alpha = (1/N^2)\sum_{ij}\langle \hat{\sigma}_i^\alpha \hat{\sigma}_j^\alpha \rangle$ in the (a) $\alpha = x$ and (b) $\alpha = z$ directions as a function of the system-bath interaction energy, λ. Other parameters are $\Delta = 0.1$, $\Omega = 10$, $J_x = 1$, $J_y = 0.9$, $J_z = 0.8$. We study chains with $N = \{4, 6, 8, 10\}$ spins; dash-dotted, dashed, and solid lines (about overlapping) correspond to $T = 0.2$, 0.1, and 0.05, respectively.

except autocorrelators, thus reaching $1/N$ at strong coupling [Fig. 2(b)]. Few other comments are in place: (i) S_α approaches zero at the asymptotically weak coupling limit due to the choice $J_\alpha > 0$. (ii) To validate results, in [52] we benchmark the mapping technique against the numerically accurate reaction-coordinate (RC) method [51,53,57,60–64]. We demonstrate an excellent agreement, particularly as N grows, even at low temperature. (iii) Given the collective nature of the coupling, the AFM to FM transition point will continue to shift to smaller λ as N grows. In contrast, the fully connected Ising model presented in Eq. (6) supports a quantum phase transition at a converged value of $\lambda > 0$, independent of N, as we show in Fig. 4.

Pairwise coupling in the Ising chain.—We examine next a simpler version of the system Hamiltonian, Eq. (2), by setting $J_y = J_z = 0$, thereby making it a quantum Ising chain. We couple the chain to a collection of baths as follows: every odd site of the chain, along with its nearest neighbor to the right, are coupled to a common bath as shown in Fig. 1(d). The total Hamiltonian is

$$\hat{H}_{\rm pair} = \hat{H}_S^{\rm Ising} + \sum_{n=1}^{N/2} \hat{S}_{{\rm pair,n}} \sum_k t_{n,k}(\hat{c}_{n,k}^\dagger + \hat{c}_{n,k}) + \sum_{n,k} \nu_{n,k} \hat{c}_{n,k}^\dagger \hat{c}_{n,k}. \quad (4)$$

Here, $\hat{H}_S^{\rm Ising} = \hat{H}_S(J_y = J_z = 0)$ and $\hat{S}_{{\rm pair},n} = \hat{\sigma}_{2n-1}^x + \hat{\sigma}_{2n}^x$; $n \in \{1, \ldots, N/2\}$ is the bath index. After the mapping [52], the effective system Hamiltonian becomes

$$\hat{H}_S^{\rm Ising,eff} = \sum_{n=1}^{N/2} (\bar{\Delta}_{2n-1}\hat{\sigma}_{2n-1}^z + \bar{\Delta}_{2n}\hat{\sigma}_{2n}^z) + \sum_{n=1}^{N/2} \left(J_x - \frac{2\lambda_{2n-1}^2}{\Omega_{2n-1}}\right)\hat{\sigma}_{2n-1}^x \hat{\sigma}_{2n}^x + \sum_{n=1}^{N/2-1} J_x \hat{\sigma}_{2n}^x \hat{\sigma}_{2n+1}^x, \quad (5)$$

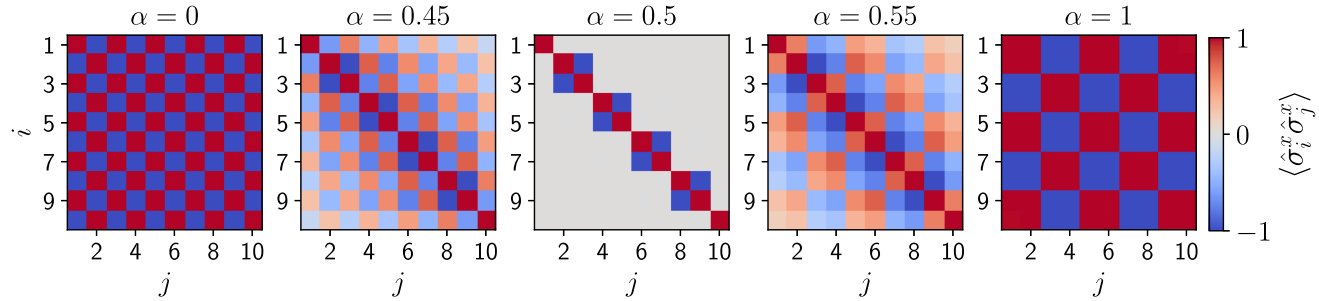

FIG. 3. Ising chain with pairwise couplings to baths. We display spin-spin correlations $\langle \hat{\sigma}_i^x \hat{\sigma}_j^x \rangle$ for $N = 10$, $\Delta = 0.1$, $J_x = 1$, $J_y = J_z = 0$, $T = 0.1$, and $\omega_c = 0.5$. Left-to-right: we increase α, the dimensionless coupling parameter in the super-Ohmic bath model. Values of α are chosen to manifest the crossover from an AFM order to an extended AFM order. Spin-spin correlations for spins coupled to the same bath precisely diminish at $\alpha = 0.5$ where we lose all long-range correlations, with the two edge spins decoupled from the rest of the chain.

where $\bar{\Delta}_{2n-1} = \Delta_{2n-1} \exp(-2\lambda_n^2/\Omega_n^2)$ and $\bar{\Delta}_{2n} = \Delta_{2n} \exp(-2\lambda_n^2/\Omega_n^2)$. We expect the two spins that are coupled to a common bath to build an FM alignment once the prefactor $[J_x - (2\lambda_{2n-1}^2/\Omega_{2n-1})]$ becomes negative at sufficiently strong coupling λ. In contrast, intercell interactions (between pairs) continue to prefer an AFM alignment, captured by the last term in Eq. (5). The combination of these two effects creates an extended Neel order at sufficiently strong coupling, where at low temperature the preferred alignment is $|\uparrow\uparrow\downarrow\downarrow\uparrow\uparrow\ldots\uparrow\uparrow\downarrow\downarrow\rangle$ in the x direction, or the opposite case.

In Fig. 3, we display spin-spin correlations $\langle \hat{\sigma}_i^x \hat{\sigma}_j^x \rangle$ for an $N = 10$-long chain. We clearly observe the buildup of spin alignments in subcells within the larger-scale AFM order as we increase the coupling parameter (left to right). As an example, we assume here super-Ohmic spectral density functions for the baths (before the mapping). As we show in [52], the pairwise ferromagnetic coupling becomes then $E_I = 2\alpha\omega_c$ (assuming identical baths). Thus, with our choice of parameters ($J_x = 1$, $\omega_c = 5\Delta$), at $\alpha = 0.5$, we precisely observe the complete suppression of long-range correlations once $J_x = 2\lambda_{2n-1}^2/\Omega_{2n-1}^2$. Furthermore, at this value the two edge spins isolate from the rest of the chain—resulting from the segmentation of the chain into pairwise sectors.

Fully connected Ising model.—We now describe a model that exhibits a bath-induced quantum phase transition (QPT) at a particular coupling strength by allowing spins to interact beyond nearest neighbor. We return to model (a) in Fig. 1, with a spin system globally coupled to a single common bath. The system's Hamiltonian is the fully connected Ising model,

$$\hat{H}_S = -\frac{\Delta}{2}\sum_{i=1}^{N} \hat{\sigma}_i^z + \frac{J\Delta}{8}\sum_{i,j=1}^{N} \hat{\sigma}_i^x \hat{\sigma}_j^x, \tag{6}$$

where $\Delta > 0$ is the spin splitting. Here, $J > 0$ is a dimensionless parameter which scales the all-to-all spin interactions in the x direction with respect to Δ. This model exhibits a QPT of a Beretzinski-Kosterlitz-Thouless (BKT) type under Ohmic dissipation as demonstrated in Ref. [2] via the quantum Monte Carlo technique. The mechanism behind this QPT is the bath induced FM interaction overcoming the intrinsic AFM interaction J. Importantly, the critical coupling strength is system size *independent* once $J \neq 0$, which allows us to identify the range of coupling strength that will retain the isolated-bath state even in the thermodynamic limit. This robustness contrasts the critical interaction scaling as $1/N$ when $J = 0$.

Our analytical mapping technique allows us to directly understand and predict this QPT from the effective Hamiltonian picture, and for general spectral functions. We couple the system (6) to a single bosonic bath and achieve the following effective system Hamiltonian [52]

$$\hat{H}_S^{\text{eff}} = -\frac{\tilde{\Delta}}{2}\sum_{i=1}^{N} \hat{\sigma}_i^z + \left(\frac{J\Delta}{8} - \frac{\lambda^2}{\Omega}\right)\sum_{i,j=1}^{N} \hat{\sigma}_i^x \hat{\sigma}_j^x. \tag{7}$$

Here, individual spin splittings Δ are suppressed to $\tilde{\Delta}$ in exactly the same manner as in Eq. (3). However, unlike the Heisenberg chain with only nearest-neighbor interactions, bath-induced FM interactions compete with the positive AFM interaction term $J\Delta$. Thus, while the example of Fig. 2 displayed a monotonic shifting of the critical coupling strength to lower values as we increase N, in the fully connected Ising model the critical coupling converges to a constant value independent of N. In Fig. 4, we demonstrate this by computing the structure factor S_x for both Brownian (a) and super-Ohmic (b) baths. The critical bath coupling $\lambda_c(\alpha_c)$ is directly obtained at the points when the original AFM order shifts to a FM order: $(J\Delta/8) = (\lambda_c^2/\Omega)$ $[(J\Delta/8) = 2\omega_c\alpha_c]$. Furthermore, we observe that the transition to a FM phase captured by S_x becomes steeper with decreasing temperature as well as an increasing number of spins, and we expect to see a discontinuous jump as $\beta, N \to \infty$ [65].

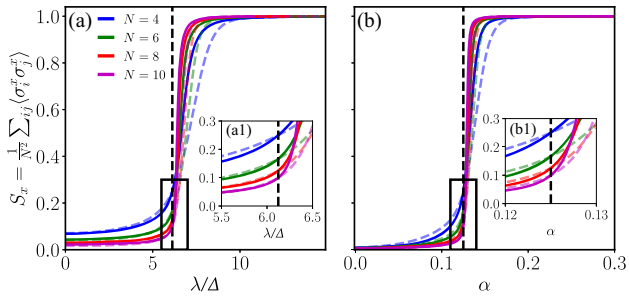

FIG. 4. Bath-induced quantum phase transition in the fully connected and globally coupled Ising model. We present the structure factor $S_x = (1/N^2)\sum_{ij}\langle\hat{\sigma}_i^x\hat{\sigma}_j^x\rangle$ using parameters corresponding to (a) Brownian (b) and a super-Ohmic spectral functions. We use $\Delta = 0.1$, $J = 3(10)$ for $a(b)$, $\Omega = 10$, and $\omega_c = 0.5$. Insets (a1) and (b1) enlarge over the corresponding main panels on the location of the quantum phase transition. Results are presented for $N = \{4, 6, 8, 10\}$ at two temperatures $T = 0.05$ (solid) and 0.1 (dashed). The dashed black line indicates where the critical $(\lambda_c)\alpha_c$ occurs, which corresponds to the point where the spin-spin interactions turn into ferromagnetic: notably, the critical coupling strength is independent of temperature and chain length (insets).

Discussion.—We showed that an analytical mapping scheme yields clear insights on dissipative phase transitions in a broad class of spin systems, shedding light on phenomena that were previously approached independently, and with costly numerical tools. The mapping takes a many-body spin Hamiltonian at potentially strong coupling to heat baths and transforms it into an effective spin model at *weak* coupling to (modified-residual) environments, for which equilibrium expectation values can be readily evaluated using the Gibbs equilibrium state. Specifically, we demonstrated that in Heisenberg chains a global bath turns a low-temperature AFM order into a FM phase; an extended Neel phase is created when pairs of spins couple to a common bath; a bath-induced QPT occurs in the fully connected Ising model. Regarding the validity of our results, one needs to operate in the regime where the system-bath coupling—in the effective Hamiltonian picture—remains weak. Furthermore, the reaction coordinate mapping assumes high-frequency baths [57,66]. As for temperatures, a comparison against more precise numerical tools [52] reveals that the mapping method progressively becomes *more accurate* with increasing chain length, even at low temperature. The mapping approach was formulated for harmonic baths, but one can generalize it to other environments, including spin baths. The scheme can also be readily generalized to higher spin systems and more complex system-bath operators. Moreover, the method lends itself to the analysis of bath-induced phases in disordered systems. With its generality and transparent form, the mapping method could be employed to design dissipation-controlled topological phases at finite temperature, the focus of our future work.

We acknowledge fruitful discussions with Yuxuan Zhang, Yong-Baek Kim, and Kartiek Agarwal. D. S. acknowledges support from an NSERC Discovery Grant and the Canada Research Chair program. The work of N. A. S. was supported by Ontario Graduate Scholarship (OGS). The work of M. B. has been supported by the Centre for Quantum Information and Quantum Control (CQIQC) at the University of Toronto. Computations were performed on the Niagara supercomputer at the SciNet HPC Consortium. SciNet is funded by the Canada Foundation for Innovation; the Government of Ontario; Ontario Research Fund–Research Excellence; and the University of Toronto.

*brett.min@mail.utoronto.ca
†dvira.segal@utoronto.ca

[1] André Winter and Heiko Rieger, Quantum phase transition and correlations in the multi-spin-boson model, Phys. Rev. B **90**, 224401 (2014).
[2] G. De Filippis, A. de Candia, A. S. Mishchenko, L. M. Cangemi, A. Nocera, P. A. Mishchenko, M. Sassetti, R. Fazio, N. Nagaosa, and V. Cataudella, Quantum phase transition of many interacting spins coupled to a bosonic bath: Static and dynamical properties, Phys. Rev. B **104**, L060410 (2021).
[3] Matthew W. Butcher, J. H. Pixley, and Andriy H. Nevidomskyy, Long-range order and quantum criticality in a dissipative spin chain, Phys. Rev. B **105**, L180407 (2022).
[4] Manuel Weber, Quantum spin chains with bond dissipation, arXiv:2310.11525.
[5] Haggai Landa, Marco Schiró, and Grégoire Misguich, Multistability of driven-dissipative quantum spins, Phys. Rev. Lett. **124**, 043601 (2020).
[6] Dolf Huybrechts, Fabrizio Minganti, Franco Nori, Michiel Wouters, and Nathan Shammah, Validity of mean-field theory in a dissipative critical system: Liouvillian gap, $\mathbb{PT}$-symmetric antigap, and permutational symmetry in the *XYZ* model, Phys. Rev. B **101**, 214302 (2020).
[7] Peter P. Orth, Ivan Stanic, and Karyn Le Hur, Dissipative quantum Ising model in a cold-atom spin-boson mixture, Phys. Rev. A **77**, 051601(R) (2008).
[8] Fa Wang and Ashvin Vishwanath, Spin phonon induced collinear order and magnetization plateaus in triangular and Kagome antiferromagnets: Applications to $CuFeO_2$, Phys. Rev. Lett. **100**, 077201 (2008).
[9] Dara P. S. McCutcheon, Ahsan Nazir, Sougato Bose, and Andrew J. Fisher, Separation-dependent localization in a two-impurity spin-boson model, Phys. Rev. B **81**, 235321 (2010).
[10] Peter P. Orth, David Roosen, Walter Hofstetter, and Karyn Le Hur, Dynamics, synchronization, and quantum phase transitions of two dissipative spins, Phys. Rev. B **82**, 144423 (2010).
[11] Vahram L. Grigoryan and Ke Xia, Cavity-mediated dissipative spin-spin coupling, Phys. Rev. B **100**, 014415 (2019).
[12] F. Iemini, A. Russomanno, J. Keeling, M. Schirò, M. Dalmonte, and R. Fazio, Boundary time crystals, Phys. Rev. Lett. **121**, 035301 (2018).

[13] Julia Hannukainen and Jonas Larson, Dissipation-driven quantum phase transitions and symmetry breaking, Phys. Rev. A **98**, 042113 (2018).

[14] H. Weisbrich, C. Saussol, W. Belzig, and G. Rastelli, Decoherence in the quantum Ising model with transverse dissipative interaction in the strong-coupling regime, Phys. Rev. A **98**, 052109 (2018).

[15] Linyu Song and Jiasen Jin, Crossover from discontinuous to continuous phase transition in a dissipative spin system with collective decay, Phys. Rev. B **108**, 054302 (2023).

[16] Xiaohui Qian, Zhe Sun, and Nengji Zhou, Unveiling quantum entanglement and correlation of sub-Ohmic and Ohmic baths for quantum phase transitions in dissipative systems, Phys. Rev. A **105**, 012431 (2022).

[17] M. Garst, S. Kehrein, T. Pruschke, A. Rosch, and M. Vojta, Quantum phase transition of Ising-coupled Kondo impurities, Phys. Rev. B **69**, 214413 (2004).

[18] G. Schehr and H. Rieger, Finite temperature behavior of strongly disordered quantum magnets coupled to a dissipative bath, J. Stat. Mech. (2008) P04012.

[19] P. Nägele, G. Campagnano, and U. Weiss, Dynamics of dissipative coupled spins: Decoherence, relaxation and effects of a spin-boson bath, New J. Phys. **10**, 115010 (2008).

[20] José A. Hoyos and Thomas Vojta, Dissipation effects in random transverse-field Ising chains, Phys. Rev. B **85**, 174403 (2012).

[21] Iver Bakken Sperstad, Einar B. Stiansen, and Asle Sudbø, Quantum criticality in spin chains with non-Ohmic dissipation, Phys. Rev. B **85**, 214302 (2012).

[22] Julius Bonart, Dissipative phase transition in a pair of coupled noisy two-level systems, Phys. Rev. B **88**, 125139 (2013).

[23] Zi Cai, Ulrich Schollwöck, and Lode Pollet, Identifying a bath-induced Bose liquid in interacting spin-boson models, Phys. Rev. Lett. **113**, 260403 (2014).

[24] G. Goldstein, C. Aron, and C. Chamon, Driven-dissipative Ising model: Mean-field solution, Phys. Rev. B **92**, 174418 (2015).

[25] Mohammad F. Maghrebi and Alexey V. Gorshkov, Nonequilibrium many-body steady states via Keldysh formalism, Phys. Rev. B **93**, 014307 (2016).

[26] Dominic C. Rose, Katarzyna Macieszczak, Igor Lesanovsky, and Juan P. Garrahan, Metastability in an open quantum Ising model, Phys. Rev. E **94**, 052132 (2016).

[27] Kabuki Takada and Hidetoshi Nishimori, Critical properties of dissipative quantum spin systems in finite dimensions, J. Phys. A **49**, 435001 (2016).

[28] Zheng Yan, Lode Pollet, Jie Lou, Xiaoqun Wang, Yan Chen, and Zi Cai, Interacting lattice systems with quantum dissipation: A quantum Monte Carlo study, Phys. Rev. B **97**, 035148 (2018).

[29] T. O. Puel, Stefano Chesi, S. Kirchner, and P. Ribeiro, Mixed-order symmetry-breaking quantum phase transition far from equilibrium, Phys. Rev. Lett. **122**, 235701 (2019).

[30] Manuel Weber, David J. Luitz, and Fakher F. Assaad, Dissipation-induced order: The $s = 1/2$ quantum spin chain coupled to an Ohmic bath, Phys. Rev. Lett. **129**, 056402 (2022).

[31] Saptarshi Majumdar, Laura Foini, Thierry Giamarchi, and Alberto Rosso, Bath-induced phase transition in a Luttinger liquid, Phys. Rev. B **107**, 165113 (2023).

[32] C. A. Perroni, A. De Candia, V. Cataudella, R. Fazio, and G. De Filippis, First-order transitions in spin chains coupled to quantum baths, Phys. Rev. B **107**, L100302 (2023).

[33] Tony E. Lee, Sarang Gopalakrishnan, and Mikhail D. Lukin, Unconventional magnetism via optical pumping of interacting spin systems, Phys. Rev. Lett. **110**, 257204 (2013).

[34] Ching-Kit Chan, Tony E. Lee, and Sarang Gopalakrishnan, Limit-cycle phase in driven-dissipative spin systems, Phys. Rev. A **91**, 051601(R) (2015).

[35] Hendrik Weimer, Variational principle for steady states of dissipative quantum many-body systems, Phys. Rev. Lett. **114**, 040402 (2015).

[36] Jiasen Jin, Alberto Biella, Oscar Viyuela, Leonardo Mazza, Jonathan Keeling, Rosario Fazio, and Davide Rossini, Cluster mean-field approach to the steady-state phase diagram of dissipative spin systems, Phys. Rev. X **6**, 031011 (2016).

[37] Masaya Nakagawa, Naoto Tsuji, Norio Kawakami, and Masahito Ueda, Dynamical sign reversal of magnetic correlations in dissipative Hubbard models, Phys. Rev. Lett. **124**, 147203 (2020).

[38] Xingli Li, Yan Li, and Jiasen Jin, Steady-state phases of the dissipative spin-1/2 XYZ model with frustrated interactions, Phys. Rev. B **104**, 155130 (2021).

[39] Vincent R. Overbeck, Mohammad F. Maghrebi, Alexey V. Gorshkov, and Hendrik Weimer, Multicritical behavior in dissipative Ising models, Phys. Rev. A **95**, 042133 (2017).

[40] R. Rota, F. Storme, N. Bartolo, R. Fazio, and C. Ciuti, Critical behavior of dissipative two-dimensional spin lattices, Phys. Rev. B **95**, 134431 (2017).

[41] E. T. Owen, J. Jin, D. Rossini, R. Fazio, and M. J. Hartmann, Quantum correlations and limit cycles in the driven-dissipative Heisenberg lattice, New J. Phys. **20**, 045004 (2018).

[42] Jiasen Jin, Alberto Biella, Oscar Viyuela, Cristiano Ciuti, Rosario Fazio, and Davide Rossini, Phase diagram of the dissipative quantum Ising model on a square lattice, Phys. Rev. B **98**, 241108(R) (2018).

[43] Julian Huber, Peter Kirton, and Peter Rabl, Nonequilibrium magnetic phases in spin lattices with gain and loss, Phys. Rev. A **102**, 012219 (2020).

[44] Daniel Jaschke, Lincoln D Carr, and Inés de Vega, Thermalization in the quantum Ising model—approximations, limits, and beyond, Quantum Sci. Technol. **4**, 034002 (2019).

[45] Tony E. Lee, H. Häffner, and M. C. Cross, Antiferromagnetic phase transition in a nonequilibrium lattice of Rydberg atoms, Phys. Rev. A **84**, 031402(R) (2011).

[46] Zejian Li, Ariane Soret, and Cristiano Ciuti, Dissipation-induced antiferromagneticlike frustration in coupled photonic resonators, Phys. Rev. A **103**, 022616 (2021).

[47] L. F. Cugliandolo, G. S. Lozano, and H. Lozza, Static properties of the dissipative random quantum Ising ferromagnetic chain, Phys. Rev. B **71**, 224421 (2005).

[48] Philipp Werner, Matthias Troyer, and Subir Sachdev, Quantum spin chains with site dissipation, J. Phys. Soc. Jpn. **74**, 67 (2005).

[49] Philipp Werner, Klaus Völker, Matthias Troyer, and Sudip Chakravarty, Phase diagram and critical exponents of a dissipative Ising spin chain in a transverse magnetic field, Phys. Rev. Lett. **94**, 047201 (2005).

[50] Nicholas Anto-Sztrikacs, Ahsan Nazir, and Dvira Segal, Effective-Hamiltonian theory of open quantum systems at strong coupling, PRX Quantum **4**, 020307 (2023).

[51] Nicholas Anto-Sztrikacs, Brett Min, Marlon Brenes, and Dvira Segal, Effective Hamiltonian theory: An approximation to the equilibrium state of open quantum systems, Phys. Rev. B **108**, 115437 (2023).

[52] See Supplemental Material at http://link.aps.org/supplemental/10.1103/PhysRevLett.132.266701 for additional information on two mapping approaches that build an analogous effective Hamiltonian for the system: (i) the reaction coordinate method followed by a polaron rotation and truncation, and (ii) the polaron transform shifting all modes in the environment. The two methods are each exercised on the four models shown in Fig. 1 to construct their effective system Hamiltonian.

[53] Ahsan Nazir and Gernot Schaller, The reaction coordinate mapping in quantum thermodynamics, in *Thermodynamics in the Quantum Regime: Fundamental Aspects and New Directions* (Springer International Publishing, New York, 2018), pp. 551–577.

[54] H. P. Breuer and F. Petruccione, *The Theory of Open Quantum Systems* (Oxford University Press, New York, 2002).

[55] J. D. Cresser and J. Anders, Weak and ultrastrong coupling limits of the quantum mean force Gibbs state, Phys. Rev. Lett. **127**, 250601 (2021).

[56] Yiu-Fung Chiu, Aidan Strathearn, and Jonathan Keeling, Numerical evaluation and robustness of the quantum mean-force Gibbs state, Phys. Rev. A **106**, 012204 (2022).

[57] Nicholas Anto-Sztrikacs and Dvira Segal, Strong coupling effects in quantum thermal transport with the reaction coordinate method, New J. Phys. **23**, 063036 (2021).

[58] Dazhi Xu and Jianshu Cao, Non-canonical distribution and non-equilibrium transport beyond weak system-bath coupling regime: A polaron transformation approach, Front. Phys. **11**, 110308 (2016).

[59] It is energetically favored for the oscillators of the bath to shift their displacements from their equilibrium position once all spins prefer a ferromagnetic alignment in the direction at which they are coupled to the common bath.

[60] Jake Iles-Smith, Neill Lambert, and Ahsan Nazir, Environmental dynamics, correlations, and the emergence of non-canonical equilibrium states in open quantum systems, Phys. Rev. A **90**, 032114 (2014).

[61] Jake Iles-Smith, Arend G. Dijkstra, Neill Lambert, and Ahsan Nazir, Energy transfer in structured and unstructured environments: Master equations beyond the Born-Markov approximations, J. Chem. Phys. **144**, 044110 (2016).

[62] Nicholas Anto-Sztrikacs and Dvira Segal, Capturing non-Markovian dynamics with the reaction coordinate method, Phys. Rev. A **104**, 052617 (2021).

[63] Nicholas Anto-Sztrikacs, Felix Ivander, and Dvira Segal, Quantum thermal transport beyond second order with the reaction coordinate mapping, J. Chem. Phys. **156**, 214107 (2022).

[64] Felix Ivander, Nicholas Anto-Sztrikacs, and Dvira Segal, Strong system-bath coupling effects in quantum absorption refrigerators, Phys. Rev. E **105**, 034112 (2022).

[65] The Brownian spectral density function behaves like an Ohmic function at low frequencies, valid when Ω is the largest energy scale in the problem. Previous studies showed that the fully connected Ising model displays a Beretzinski-Kosterlitz-Thouless (BKT) QPT in this model [2]. This QPT can be characterized by the squared magnetization as the order parameter.

[66] While broadly speaking, the mapping relies on operating in the limit of $\Omega > \lambda$, as well as $\Omega \gg \Delta, J$ [57], we found analytically [50], and through comparison to a numerically exact method [51] that results of the effective model were accurate beyond that, and even in the asymptotically large λ. This is due to the fact that model parameters in the effective Hamiltonian are normalized such that they approach a constant value at asymptotically large λ, rather than diverging with λ, see also Sec. S2.A in [52].